The final publication is available at

https://doi.org/10.1115/1.4037405

Additional Information

Strain-level dependent non-equilibrium anisotropic viscoelasticity: Application to the abdominal muscle

Marcos Latorre[*]
Escuela Técnica Superior de Ingeniería Aeronáutica y del Espacio
Universidad Politécnica de Madrid
Plaza Cardenal Cisneros, 3, 28040-Madrid, Spain
Email: m.latorre.ferrus@upm.es

Francisco J. Montáns
Escuela Técnica Superior de Ingeniería Aeronáutica y del Espacio
Universidad Politécnica de Madrid
Plaza Cardenal Cisneros, 3, 28040-Madrid, Spain
Email: fco.montans@upm.es

Soft connective tissues sustain large strains of viscoelastic nature. The rate-independent component is frequently modelled by means of anisotropic hyperelastic models. The rate-dependent component is usually modelled through linear rheological models or quasilinear viscoelastic models. These viscoelastic models are unable, in general, to capture the strain-level dependency of the viscoelastic properties present in many viscoelastic tissues. In linear viscoelastic models, strain-level dependency is frequently accounted for by including the dependence of multipliers of Prony series on strains through additional evolution laws, but the determination of the material parameters is a difficult task and the obtained accuracy is usually not sufficient. In this work we introduce a model for fully nonlinear viscoelasticity in which the instantaneous and quasistatic behaviors are exactly captured and the relaxation curves are predicted to a high accuracy. The model is based on a fully nonlinear standard rheological model and does not necessitate optimization algorithms to obtain material parameters. Furthermore, in contrast to most models used in modelling the viscoelastic behavior of soft tissues, it is valid for the large deviations from thermodynamic equilibrium typically observed in soft tissues.

1 Introduction

The actual behavior of soft biological tissues has a relevant viscous, rate-dependent component [1], [2]. The modelling of viscoelastic effects in soft tissues commonly follows two approaches. The first approach consists of using integral equations in some of the available forms: nonlinear superposition, Schapery, or Quasilinear Viscoelasticity (QLV), see [1], [3]. Quasilinear Viscoelasticity is a common approach mainly in the unidimensional modeling of soft tissues [1] and with nonlinear hypoelastic or linearized anisotropic

elastic models of soft tissues [4], [5], [6]. For the three dimensional treatment of viscoelasticity of soft tissues for finite element implementation, the differential approach formulated by Simó [7] (see also [8] and therein references), which is valid for anisotropy, seems to be the most common approach because of its numerical efficiency thanks to a recurrence numerical formula [8] so only the information of the previous step is needed. This approach, with small modifications, is followed by many authors when modelling soft tissues; [8], [9], [10], [11], [12], [13], [14]. These works are not compatible in general with the well-accepted multiplicative decompositions [7]. Furthermore, as noted by several authors (see for example Holzapfel [12], Section 6.10, Reese and Govindjee [15], Haslach [16], Haupt [17], among others) both quasilinear viscoelasticity and the large strain formulations based on the Simó approach, named *quasi*-equilibrium viscoelasticity or finite *linear* viscoelasticity [15], are useful for large strains, but only for small deviations from thermodynamic equilibrium.

Soft biological tissues show stress relaxation ratios that depend on the strain level, a dependence which is different for different tissues, as it can be clearly seen for example in [10], [3], [18] among others. Therefore, from a practical standpoint regarding the analysis of soft tissues with models amenable of being implemented in implicit finite element programs (to model general geometries and loading conditions), finite *linear* viscoelasticity results in the known difficulties in capturing naturally both the strain dependence of the viscous behavior in soft tissues (e.g. the resulting relaxation curves) and the shape of those curves, see for example [10], [19], [18]. It is obvious that if the simplest relaxation tests are not properly predicted, any finite element simulation of the viscoelastic behavior of soft tissues under general loading conditions (for example when simulating surgery) will have at least similar inaccuracies. A minimum requirement should be to capture at least these simplest tests defining the

---

[*]Address all correspondence to this author.

material behavior to good accuracy because, otherwise, confidence in finite element simulations cannot be obtained.

On the other side, the so-called *non*-equilibrium viscoelasticity or finite *nonlinear* viscoelasticity [15], (1) allows for the unrelated instantaneous and equilibrated hyperelastic behaviors observed in soft biological tissues, (2) non-equilibrated elastic strains come from a multiplicative decomposition and may effectively be of the order of the total strains, representing large deviations from thermodynamical equilibrium, as observed in tests, (3) the evolution equation for those internal strains is fully nonlinear, governed by the hyperelastic behavior of the non-equilibrated part, which is also the dissipation potential, and (4) at every instant, stresses are formally derived from a total stored energy. In contrast, in *quasi*-equilibrium viscoelasticity (either based on the Simó approach or on the QLV one) the evolution of the internal variables is governed by a *linear* differential equation established at the *quasi*-equilibrium point, so instantaneous and equilibrated responses are in principle proportional, as in the infinitesimal case [8], [12], non-equilibrated strains should be moderate [15], [12], and stresses are not derived from a stored energy, except at the instantaneous or equilibrium states. Indeed, these properties clearly explain why strain-dependent relaxation tests in soft biological tissues are not properly captured using these traditional, popular models.

The purpose of this paper is to present a new model for the viscoelastic behavior of soft tissues under large *non*-equilibrated elastic deformations which naturally accounts for fully nonlinear, strain-dependent *non*-equilibrium viscoelasticity, and is amenable of finite element implementation to model general geometries and loading conditions found when simulating, for example, surgery in organs. The model is based on the kinematics and finite element algorithmic implementation of non-equilibrium anisotropic viscoelasticity [20], [21], originally developed for isotropic behavior by Reese and Govindjee [15]. The main ingredient introduced herein is the consideration of viscous parameters that depend on the non-equilibrium deformation level. This approach, based on a different thermodynamic treatment, has proved very useful when modeling viscoelastic elastomers at high strain rates [22–24]. For the hyperelastic behavior part, we use What-You-Prescribe-Is-What-You-Get (WYPiWYG) hyperelasticity [25], [26], [27], which has accurately predicted the passive behavior of a large variety of soft tissues, like skeletal muscle [28], fascia [29], skin [30], arteries [31], myocardium [32] and herein abdominal muscle. The model presented herein is based on a physically-sound thermodynamic framework, has unparalleled accuracy and does not require optimization or any complex procedure to determine any material parameter. All the information needed is immediately obtained from the available experimental data.

2 WYPiWYG hyperelasticity

WYPiWYG hyperelasticity is a data-driven, model-free constitutive modelling technique for obtaining numerically the stored energy of soft materials directly from experimental tests, without user intervention. In contrast to most models used in modelling anisotropic soft tissues, WYPiWYG hyperelasticity is compatible with the equivalent infinitesimal theory, not only at the reference configuration [33], but at

all deformation levels, so physical insight is easily obtained during finite strain analyses [30, 31]. Consider the polar decomposition of the deformation gradient $\mathbf{X}$ as

$$\mathbf{X} = \mathbf{RU} \tag{1}$$

where $\mathbf{R}$ is the rotation tensor and $\mathbf{U}$ is the stretch tensor in the material basis. The material logarithmic strain tensor is $\mathbf{E} = \ln \mathbf{U}$, which principal components $E_i = \ln \lambda_i$ are the logarithms of the principal stretches λ_i. Since soft tissues behavior may be considered isochoric, we will assume that $J = \det(\mathbf{X}) = 1$, so the deviatoric part of $\mathbf{E}$ is coincident with $\mathbf{E}$, i.e. $\mathbf{E}^d = \mathbb{P}^S : \mathbf{E} \equiv \mathbf{E}$, where $\mathbb{P}^S$ is the (small-strain-equivalent) fourth-order deviatoric projection tensor in the logarithmic strain space, with Cartesian components in terms of the Kronecker delta δ_{ij}

$$\left(\mathbb{P}^S\right)_{ijkl} = \frac{1}{2}(\delta_{ik}\delta_{jl} + \delta_{il}\delta_{jk}) - \frac{1}{3}\delta_{ij}\delta_{kl} \tag{2}$$

WYPiWYG hyperelasticity for incompressible orthotropic materials (as an example) is based on the following decomposition [34]

$$\mathcal{W}\left(\mathbf{E}^d, \mathbf{a}_1, \mathbf{a}_2\right) = \mathcal{W}_{iso}\left(\mathbf{E}^d\right) + \mathcal{W}_{orth}\left(\mathbf{E}^d, \mathbf{a}_1, \mathbf{a}_2\right) \tag{3}$$

with $\mathcal{W}_{iso}\left(\mathbf{E}^d\right)$ being the isotropic contribution following the Valanis-Landel decomposition

$$\mathcal{W}_{iso}\left(\mathbf{E}^d\right) = \omega\left(E_1^d\right) + \omega\left(E_2^d\right) + \omega\left(E_3^d\right) \tag{4}$$

and $\mathcal{W}_{orth}\left(\mathbf{E}^d, \mathbf{a}_1, \mathbf{a}_2\right)$ is an orthotropic contribution for preferred material directions $\mathbf{a}_i$, which follows a decomposition similar to that found in the infinitesimal setting (although the most general coupled form is also possible [32])

$$\mathcal{W}_{orth}\left(\mathbf{E}^d, \mathbf{a}_1, \mathbf{a}_2\right) = \omega_{11}\left(E_{11}^d\right) + \omega_{22}\left(E_{22}^d\right) + \omega_{33}\left(E_{33}^d\right) \\ + 2\omega_{12}\left(E_{12}^d\right) + 2\omega_{23}\left(E_{23}^d\right) + 2\omega_{31}\left(E_{31}^d\right) \tag{5}$$

where $\mathbf{a}_i$ are the principal material directions perpendicular to the planes of symmetry, E_i^d are the principal *isochoric* logarithmic strains, $E_{ij}^d = \mathbf{a}_i \cdot \mathbf{E}^d \cdot \mathbf{a}_j$ are the components of the *deviatoric* logarithmic material strain tensor $\mathbf{E}^d$ in the preferred material directions and $\omega(E^d)$ and $\omega_{ij}(E_{ij}^d)$ are functions determined by the WYPiWYG computational procedure. The global shape of these functions is not given beforehand, but computed numerically solving the differential equations associated with the experiments and performing a spline interpolation between exactly computed strain energy values. The resulting function is a piecewise smooth analytical function. As in the infinitesimal setting, only the coupled shear invariant $E_{12}^d E_{23}^d E_{31}^d$ is neglected [26]. The actual computational procedure for these functions for the different symmetry cases is given in [25], [28], [26], [34], [27]. A general

procedure without inversion formula with application to the Dokos et al. shear experiments on myocardium [35] can be found in [32]. Obviously, because the WYPiWYG formulation preserves analytical and numerical material symmetries congruency [34], the isotropic behavior is just a particular case recovered numerically if the curves correspond to those of an isotropic material.

For the matter of simplicity in the exposition, and without loss of generality of the presented formulation, we assume hereafter that $\mathcal{W} \equiv \mathcal{W}_{orth}$. For further reference, we note that the work-conjugate stress tensor of the material logarithmic strain tensor is the generalized Kirchhoff stress tensor obtained through [36]—for simplicity of notation we omit the material directions in the dependencies

$$\mathbf{T} = \frac{d\mathcal{W}\left(\mathbf{E}^d\right)}{d\mathbf{E}} + p\mathbf{I} = \mathbf{T}^d + p\mathbf{I} \qquad (6)$$

where p is the Lagrange multiplier enforcing the incompressibility condition and we define the purely deviatoric stresses

$$\mathbf{T}^d := \frac{d\mathcal{W}\left(\mathbf{E}^d\right)}{d\mathbf{E}} = \frac{d\mathcal{W}\left(\mathbf{E}^d\right)}{d\mathbf{E}^d} : \frac{d\mathbf{E}^d}{d\mathbf{E}} = \sum_{i=1}^{3}\sum_{j=1}^{3} \omega'_{ij}(E^d_{ij})\mathbf{L}^S_{ij} : \mathbb{P}^S$$

where $\mathbf{L}^S_{ij} = \frac{1}{2}(\partial E^d_{ij}/\partial\mathbf{E}^d + \partial E^d_{ji}/\partial\mathbf{E}^d) = \frac{1}{2}\left(\mathbf{a}_i \otimes \mathbf{a}_j + \mathbf{a}_j \otimes \mathbf{a}_i\right)$ are orthotropy structural tensors and the projection tensor $\mathbb{P}^S = d\mathbf{E}^d/d\mathbf{E}$ has been defined above. A subsequent differentiation gives—see details in [26], [36]

$$\frac{d\mathbf{T}^d}{d\mathbf{E}} = \frac{d^2\mathcal{W}\left(\mathbf{E}^d\right)}{d\mathbf{E}d\mathbf{E}} = \frac{d\mathbf{E}^d}{d\mathbf{E}} : \frac{d^2\mathcal{W}\left(\mathbf{E}^d\right)}{d\mathbf{E}^d d\mathbf{E}^d} : \frac{d\mathbf{E}^d}{d\mathbf{E}}$$
$$= \mathbb{P}^S : \sum_{i=1}^{3}\sum_{j=1}^{3} \omega''_{ij}(E^d_{ij})\mathbf{L}^S_{ij} \otimes \mathbf{L}^S_{ij} : \mathbb{P}^S \qquad (7)$$

Note that in the usual quasi-incompressible case employed in finite element analyses, the volumetric stresses $p\mathbf{I}$ are conveniently computed by means of an explicit penalty volumetric strain energy term and mixed finite element formulations are required [26].

3 Finite fully nonlinear, non-equilibrium anisotropic viscoelasticity

Non-equilibrium viscoelasticity allows for arbitrarily large deviations from thermodynamic equilibrium, i.e. large unbalanced internal elastic strains. These large unbalanced deformations are present when a biological tissue is subjected to a fast change of strains, and the corresponding overstresses change significantly in time during the corresponding relaxation. During that relaxation, an important part of the initially stored energy is dissipated. Quasi-equilibrium and quasilinear viscoelasticity assume implicitly that the internal deformations are not too away from the equilibrium state, so for example, during relaxation tests, that equilibrium state characterizes the dissipation during the test. As a practical consequence, the resulting dissipated energy is (linearly) proportional to the equilibrium stored energy, i.e. instantaneous

and quasistatic stress-strain responses are proportional, and relaxation curves are independent of the strain level. This is in contradiction to the experimental observation in many soft tissues, see for example [10], [19], [3], [18].

To accommodate experimental observations in a simple, yet sound framework amenable of efficient finite element implementation, Lubliner [37], motivated by the standard rheological model, see Figure 1, proposed the existence of an equilibrated $\mathcal{W}_{eq}$ and a nonequilibrated energy $\mathcal{W}_{neq}$ (the energies stored in the springs of the rheological model in Fig. 1). Departing from an unloaded configuration, during deformations at a relevant speed relative to a characteristic relaxation time, we have $\mathbf{E}_e \approx \mathbf{E}$ and the initial stored energy is the addition of both for the given strains, i.e. $\mathcal{W} = \mathcal{W}_{eq}(\mathbf{E}^d) + \mathcal{W}_{neq}(\mathbf{E}^d_e)$. On other side, during quasistatic deformations $\mathbf{E}_e \approx \mathbf{0}$, so the stored energy is given by $\mathcal{W}_{eq}(\mathbf{E}^d)$. The stress power $\mathcal{P}$ is

$$\mathcal{P} = \dot{\mathcal{W}}_{eq} + \dot{\mathcal{W}}_{neq} + \mathcal{D} \qquad (8)$$

During a relaxation test at a fixed strain level $\mathbf{E}$, $\mathcal{P} = 0$, $\dot{\mathcal{W}}_{eq} = 0$, so $\mathcal{D} = -\dot{\mathcal{W}}_{neq}$, and the stored energy $\mathcal{W}_{eq} + \mathcal{W}_{neq}$ relaxes to $\mathcal{W}_{eq}$, dissipating the nonequilibrated energy $\mathcal{W}_{neq}$. Hence the dissipated energy and the equilibrated energy are fully uncoupled and both energies can be determined directly from experimental tests. In fact, the nonequilibrated energy is the potential of dissipation, so if the external deformations are fixed, both the final state (through $\mathcal{W}_{eq}$) and the dissipation from $t = 0$ to $t \to \infty$ (through $\mathcal{W}_{neq}$) are known beforehand. Remarkably, the response is hyperelastic at all times, meaning that stresses are always derived from a stored energy (say isochronic) function, see Figure 1. Using WYPiWYG hyperelasticity, energies and hence dissipation are determined in a numerically exact way, so both the nonequilibrated (fast) and quasiequilibrium (either slow or relaxed) behaviors, as well as the total energy dissipated, are captured to a high accuracy.

The best-known computational framework based on equilibrated and nonequilibrated energies is the model of Reese and Govindjee [15], which was formulated for isotropic materials. We have recently extended the model for anisotropic materials [20], [21]. Remarkably, the new formulation, which reduces to the Reese and Govindjee model for the special case of isotropy, is even simpler, using a *conventional* viscous flow rule in the logarithmic strain space that adopts the same form as the viscous flow rule in the small strain case. The present formulation is based on the works presented in [20], [21]. However, the formulations in [20], [21] do not incorporate strain-dependent viscous behavior. Then, as initially proposed, this results in the lack of ability to control the isochronic curves, or equivalently, the rate at which dissipation takes place for a given initial deformation. As mentioned, in soft biological tissues, the relaxation curves, and hence the normalized dissipation rates, depend on initial strains [10], [19], [3], [18]. In this work we adapt the framework to account for the strain dependency of viscosity properties observed in soft tissues. Importantly, the same issue was solved in a similar way when modeling the viscoelastic behavior of elastomers at high strain rates, see [22–24].
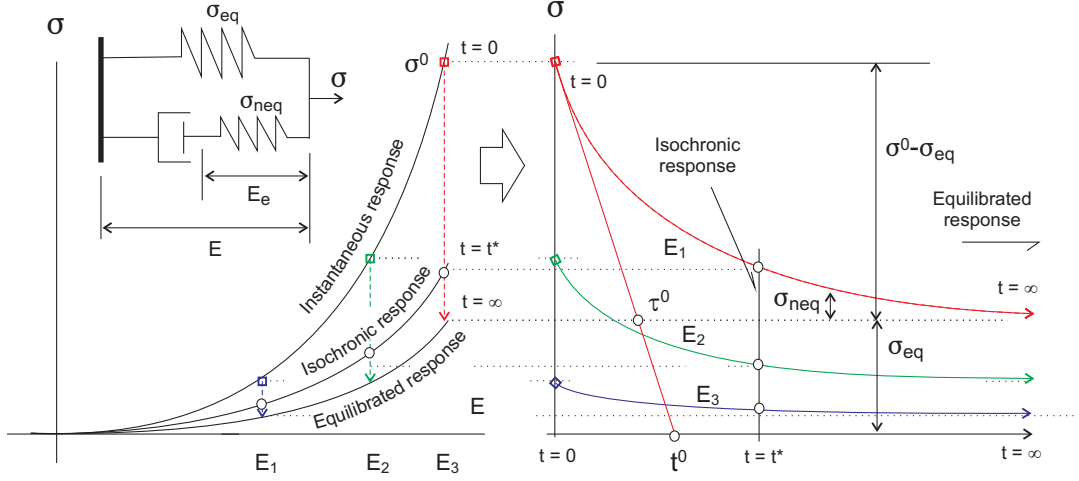
Fig. 1. a) Stress-strain behavior under instantaneous loads; equilibrated, relaxed response and isochronic response. b) Relaxation tests.

The viscoelastic formulations in [20], [21] are based on the well-accepted multiplicative decompositions of the total deformation gradient $\mathbf{X}$ into an elastic (nonequilibrated) and a viscous part

$$\text{either} \qquad \mathbf{X} = \mathbf{X}_e \mathbf{X}_v \qquad \text{or} \qquad \mathbf{X} = \mathbf{X}_v \mathbf{X}_e \qquad (9)$$

The former is known as the Sidoroff decomposition. These multiplicative decompositions conceptually establish the existence of a local, thermodynamically unbalanced deformation given by $\mathbf{X}_e$, which is of isochoric nature, $\det(\mathbf{X}_e) = 1$, and relaxes nonlinearly in time according to the corresponding nonlinear, unbalanced stored energy. We refer the readers to Refs. [20] and [21] for details on both formulations and their algorithmic, finite element implementations. In connective tissues like perimysium (with organized cross-ply collagen fibre arrangement) or skin (with a more disperse collagen arrangement) the viscoelastic mechanism seems to reside within the collagen fibres or at the interface between fibre and matrix [38]. Therefore, no relevant reorientation of collagen fibers is apparent [38] and the symmetry group may be considered fixed during stress relaxation.

The energy dependencies are established in terms of the material logarithmic strains of the respective deformation gradients

$$\mathbf{E}_e = \ln(\mathbf{U}_e) \qquad \text{and} \qquad \mathbf{E} = \ln(\mathbf{U}) \qquad (10)$$

with $\mathbf{E}^d = \mathbb{P}^S : \mathbf{E} \equiv \mathbf{E}$ and where $\mathbf{U}_e$ is the right stretch tensor of the elastic (nonequilibrated) deformation gradient, see motivation in Figure 1. Since the internal response is purely isochoric as well, we also have $\mathbf{E}_e^d = \mathbb{P}^S : \mathbf{E}_e \equiv \mathbf{E}_e$. The total (distortional) energy is given by

$$\mathcal{W}(\mathbf{E}^d, \mathbf{E}_e^d) = \mathcal{W}_{eq}(\mathbf{E}^d) + \mathcal{W}_{neq}(\mathbf{E}_e^d) \qquad (11)$$

where, taking for instance the Sidoroff decomposition in Eq. (9), we consider $\mathbf{E}_e^d$ as an internal (dependent) variable determined from the external strains $\mathbf{E}^d$ and the internal deforma-

tions $\mathbf{X}_v$ (considered the independent kinematic variables)

$$\mathbf{E}_e^d = \mathbf{E}_e^d(\mathbf{E}^d, \mathbf{X}_v) \qquad (12)$$

The deviatoric part of the total generalized Kirchhoff stress tensor is obtained from the usual Coleman procedure, which using the Sidoroff decomposition is —see details in [20]

$$\begin{aligned} \mathbf{T}^d &= \frac{\partial \mathcal{W}(\mathbf{E}^d, \mathbf{X}_v)}{\partial \mathbf{E}} = \mathbf{T}_{eq}^d + \mathbf{T}_{neq}^d \\ &= \underbrace{\frac{d\mathcal{W}_{eq}(\mathbf{E}^d)}{d\mathbf{E}^d} : \mathbb{P}^S}_{\mathbf{T}_{eq}^d} + \underbrace{\frac{d\mathcal{W}_{neq}(\mathbf{E}_e^d)}{d\mathbf{E}_e^d} : \mathbb{P}^S}_{\mathbf{T}_{neq}^{|e}} : \left. \frac{\partial \mathbf{E}_e}{\partial \mathbf{E}} \right|_{\dot{\mathbf{X}}_v = \mathbf{0}} \end{aligned} \qquad (13)$$

where $\partial \mathbf{E}_e / \partial \mathbf{E}|_{\dot{\mathbf{X}}_v = \mathbf{0}}$ stands for the corresponding fourth-order partial derivative tensor of $\mathbf{E}_e^d(\mathbf{E}^d, \mathbf{X}_v)$, which we obtain in the next section, and we note that both $\mathbf{T}_{eq}^d$ and $\mathbf{T}_{neq}^{|e}$ are purely deviatoric by construction. We see just below that $\mathbf{T}_{neq}^{|e}$ are the relevant deviatoric nonequilibrated generalized Kirchhoff stresses. For the case of isochoric axial deformations along the principal symmetry material axes, the generalized Kirchhoff stresses $\mathbf{T}^d$ are coincident with the deviatoric Cauchy stresses σ^d, which is a very convenient modelling feature [36]. The flow rule in the formulations given in [20] and [21] ensures positive dissipation $\mathcal{D} > 0$ and adopts the following conventional form in terms of logarithmic strains and nonequilibrated stresses

$$-\dot{\mathbf{E}}_e\big|_{\dot{\mathbf{E}} = \mathbf{0}} = \mathbb{V}^{-1} : \mathbf{T}_{neq}^{|e} \qquad (14)$$

where $\dot{\mathbf{E}}_e|_{\dot{\mathbf{E}} = \mathbf{0}}$ is the partial contribution to the total rate $\dot{\mathbf{E}}_e$ when the total deformation is fixed, i.e. during the purely dissipative correction evolution. We refer to Equation (14) as a *mixed-field evolution equation* because it relates strain rates to stress values. Indeed, for rotationless cases for which $\mathbf{E}_e = \mathbf{E} - \mathbf{E}_v$ is exact, with $\mathbf{E}_v = \ln \mathbf{U}_v$, Eq. (14) specializes to

the following small-strain-equivalent expression

$$\dot{\mathbf{E}}_v = \mathbb{V}^{-1} : \mathbf{T}_{neq}^{|e} \qquad (15)$$

which is nothing but the constitutive equation of an equivalent three-dimensional dashpot in principal directions relating its internal viscous strain rates and stresses. However, Eq. (14) is six-dimensional and valid for the most general anisotropic case under arbitrary deformations of the type $\mathbf{E}_e = \mathbf{E}_e(\mathbf{E}, \mathbf{X}_v)$. The tensor $\mathbb{V}$ is an orthotropic deviatoric tensor of viscosities, which is, in general, deformation-dependent

$$\mathbb{V}^{-1}\left(\mathbf{E}_e^d\right) = \mathbb{P}^S : \left(\sum_{i=1}^{3}\sum_{j=1}^{3} \frac{1}{2\eta_{ij}^d\left(\mathbf{E}_e^d\right)}\mathbf{L}_{ij}^S \otimes \mathbf{L}_{ij}^S\right) : \mathbb{P}^S$$
$$= \mathbb{P}^S : \bar{\mathbb{V}}^{-1}\left(\mathbf{E}_e^d\right) : \mathbb{P}^S \qquad (16)$$

where $\eta_{ij}^d(\mathbf{E}_e^d)$ are the orthotropic viscosities and the tensor $\bar{\mathbb{V}}^{-1}(\mathbf{E}_e^d)$ is "diagonal" in matrix representation in preferred axes. For the viscous isotropy case, $\mathbb{V}^{-1}(\mathbf{E}_e^d)$ simplifies to

$$\mathbb{V}^{-1}\left(\mathbf{E}_e^d\right) = \frac{1}{2\eta^d\left(\mathbf{E}_e^d\right)}\mathbb{P}^S \qquad (17)$$

Equation (14) is a fully nonlinear viscous evolution equation in which the viscous flow (i.e. either $-\dot{\mathbf{E}}_e|_{\dot{\mathbf{E}}=0}$ in the most general case or $\dot{\mathbf{E}}_v$ in some particular cases) depends on both the deformation-dependent viscosity tensor $\mathbb{V}^{-1}(\mathbf{E}_e^d)$ and the thermodynamically unbalanced nonlinear energy through $\mathbf{T}_{neq}^{|e} = d\mathcal{W}_{neq}(\mathbf{E}_e^d)/d\mathbf{E}_e$. However, based on the original work [15], we considered constant viscosities in Refs. [20] and [21], which implies that even though the viscous evolution is still strain-dependent through $\mathbf{T}_{neq}^{|e}$, the shape of the relaxation curves, as well as the apparent relaxation times are already determined by $d\mathcal{W}_{neq}(\mathbf{E}_e^d)/d\mathbf{E}_e$, so the model cannot capture adequately the experimental observations in soft tissues, in general.

Considering the case with deformation-dependent viscosities, the formal application of the chain rule gives the following *single-field evolution equation* relating stress rates to stress values

$$\dot{\mathbf{T}}_{neq}^{|e}\Big|_{\dot{\mathbf{E}}=0} = \frac{d^2\mathcal{W}_{neq}}{d\mathbf{E}_e d\mathbf{E}_e} : \dot{\mathbf{E}}_e\big|_{\dot{\mathbf{E}}=0} = -\mathbb{T}^{-1}\left(\mathbf{E}_e^d\right) : \mathbf{T}_{neq}^{|e} \quad (18)$$

where we have used Eq. (14) and we identify

$$\mathbb{T}^{-1}\left(\mathbf{E}_e^d\right) := \frac{d^2\mathcal{W}_{neq}\left(\mathbf{E}_e^d\right)}{d\mathbf{E}_e d\mathbf{E}_e} : \mathbb{V}^{-1}\left(\mathbf{E}_e^d\right) \qquad (19)$$

as a fourth-order tensor including deformation-dependent relaxation times. Note that $\mathbb{T}^{-1}$ inherits, by construction, the deviatoric nature from both $d^2\mathcal{W}_{neq}/d\mathbf{E}_e d\mathbf{E}_e$ and $\mathbb{V}^{-1}$, i.e.

$$\mathbb{T}^{-1}\left(\mathbf{E}_v^d\right) = \mathbb{P}^S : \bar{\mathbb{T}}^{-1}\left(\mathbf{E}_e^d\right) : \mathbb{P}^S \qquad (20)$$

with—see Eqs. (7) and (16)

$$\bar{\mathbb{T}}^{-1}\left(\mathbf{E}_e^d\right) = \frac{d^2\mathcal{W}_{neq}\left(\mathbf{E}_e^d\right)}{d\mathbf{E}_e^d d\mathbf{E}_e^d} : \mathbb{P}^S : \bar{\mathbb{V}}^{-1}\left(\mathbf{E}_e^d\right) \qquad (21)$$

For illustrative purposes, consider the case with orthotropic hyperelasticity combined with isotropic viscosity (cf. Eqs. (7) and (17)). The tensor $\mathbb{T}^{-1}(\mathbf{E}_e^d)$ reads in this case

$$\mathbb{T}^{-1}\left(\mathbf{E}_e^d\right) = \mathbb{P}^S : \sum_{i=1}^{3}\sum_{j=1}^{3} \frac{1}{\tau_{ij}\left(\mathbf{E}_e^d\right)}\mathbf{L}_{ij}^S \otimes \mathbf{L}_{ij}^S : \mathbb{P}^S \qquad (22)$$

where we readily identify the nonequilibrium-strain-dependent relaxation time functions

$$\tau_{ij}\left(\mathbf{E}_e^d\right) = \frac{2\eta^d\left(\mathbf{E}_e^d\right)}{\omega_{neq\ ij}''\left(\mathbf{E}_e^d\right)} \qquad (23)$$

where $\omega_{neq\ ij}''(\mathbf{E}_e^d)$ are the second derivatives of the components of the nonequilibrated strain energy. What we want to illustrate in Eq. (23) is that the relaxation times of the resulting model depend on both deformation-dependent viscosities and deformation-dependent elasticity moduli. On the one hand, the consideration of deformation-dependent elasticity in both the equilibrated and non-equilibrated parts (in particular, WYPiWYG hyperelasticity) will allow us to exactly capture the instantaneous and quasi-static responses, which is equivalent to capture the different peak/relaxed stress ratios at different strain levels in relaxation tests, see Figure 1. On the other hand, the consideration of deformation-dependent viscosity parameters will allow us to capture the different relaxation evolutions at different strain levels, which is equivalent to capture the different isochronic responses obtained at different rates, see Figure 1. Importantly, we will be able to reproduce all these responses to a high accuracy using a single nonequilibrated Maxwell element, see Figure 1. Finally, it is apparent that if the relaxation times τ_{ij} are considered constant, then the stress evolutions given by Eq. (18) follow an exponential decay during relaxation tests, as expected.

4 Determination of the deformation-dependent viscosities from experimental data

The modifications in the formulations of Refs. [20] and [21] as given above facilitate the use of the present framework to accurately model soft biological tissues. In the present framework, the shape of the relaxation curves, as well as strain-level dependency, are naturally captured without the use of additional material parameters. In the following subsections we explain how to determine the viscosities $2\eta_{ij}^d(\mathbf{E}_e^d)$ from experimental data, which are the material parameters defining the viscous response in our computational models, see Eqs. (14) and (16).

4.1 Isotropic case

Assume a uniaxial relaxation test over an isotropic incompressible material. In this isochoric rotationless case,

generalized Kirchhoff stresses $\mathbf{T}$, Kirchhoff stresses τ and Cauchy stresses σ are coincident [36]. Since the longitudinal stretch is fixed, so are the lateral ones. The pressure changes because the corresponding stress does. The principal components of the stresses, with equilibrated and non-equilibrated contributions written in terms of uniaxial-equivalent deviatoric stresses are—cf. Eq. (13) with $\partial \mathbf{E}_e/\partial \mathbf{E}|_{\dot{\mathbf{X}}_v = \mathbf{0}} = \partial(\mathbf{E} - \mathbf{E}_v)/\partial \mathbf{E}$ exactly specializing to the fourth-order identity tensor in this particular case

$$
\begin{bmatrix} \sigma(t) \\ 0 \\ 0 \end{bmatrix} = \underbrace{\begin{bmatrix} \frac{2}{3}\sigma_{eq} \\ -\frac{1}{3}\sigma_{eq} \\ -\frac{1}{3}\sigma_{eq} \end{bmatrix}}_{\sigma_{eq}^d} + \underbrace{\begin{bmatrix} \frac{2}{3}\sigma_{neq}(t) \\ -\frac{1}{3}\sigma_{neq}(t) \\ -\frac{1}{3}\sigma_{neq}(t) \end{bmatrix}}_{\sigma_{neq}^d = \sigma_{neq}^{|e}} + \begin{bmatrix} p(t) \\ p(t) \\ p(t) \end{bmatrix} \quad (24)
$$

where the equilibrated contribution σ_{eq} to the uniaxial Cauchy stress $\sigma(t)$ remains constant during the relaxation test. From the second equation we obtain the evolution of the pressure

$$
p(t) = \tfrac{1}{3}(\sigma_{eq} + \sigma_{neq}(t)) \quad (25)
$$

and we substitute in the first equation to get the expected relation

$$
\sigma(t) = \sigma_{eq} + \sigma_{neq}(t) \quad (26)
$$

Equation (14) for $t > 0^+$ specializes to —note that $\dot{\mathbf{E}}(t > 0^+) = \mathbf{0}$, i.e. the external instantaneous deformation is applied during the interval $0 \leq t \leq 0^+$ and then it is retained, and that $\mathbb{P}^S : \sigma_{neq}^{|e} = \sigma_{neq}^{|e}$

$$
\dot{\mathbf{E}}_e|_{\dot{\mathbf{E}}=\mathbf{0}} \equiv \dot{\mathbf{E}}_e = -\frac{1}{2\eta^d(\|\mathbf{E}_e\|)}\sigma_{neq}^{|e} \quad (27)
$$

where, in order to obtain a dependence of general validity, we should consider η^d as a function of the invariants of $\mathbf{E}_e$, e.g. we assume that η^d depends on the norm of $\mathbf{E}_e$. Noticing that the principal components of $\mathbf{E}_e$ are

$$
[\mathbf{E}_e] = \begin{bmatrix} E_e \\ -\frac{1}{2}E_e \\ -\frac{1}{2}E_e \end{bmatrix} \quad (28)
$$

Eq. (27) reduces in the uniaxial axis to

$$
\dot{E}_e(t) = -\frac{\sigma_{neq}(t)}{3\eta^d(\|\mathbf{E}_e(t)\|)} \quad (29)
$$

with $\|\mathbf{E}_e\| = \sqrt{3}E_e/2$. Note that Equation (29) is a *fully nonlinear* mixed-field constitutive equation relating nonequilibrated stresses and viscous strain rates (note that in this particular case $\dot{E}_v = -\dot{E}_e$ and that both σ_{neq} and η^d are nonlinear

functions of E_e). It is straightforward to obtain from Eq. (18)

$$
\dot{\sigma}_{neq}(t) = -\frac{\sigma_{neq}(t)}{\tau(\|\mathbf{E}_e(t)\|)} \quad (30)
$$

which is the truly single-stress-field differential equation of the relaxation test.

In a strain-driven setup ideal for finite element analysis, however, the modification of the models of Refs. [20] and [21] is conceptually simple if we determine $\eta^d(\|\mathbf{E}_e\|)$. In order to do so, consider the nonequilibrated over-stress evolution $\sigma_{neq}(t) = \sigma(t) - \sigma_{eq}$ during a given relaxation test (see Figure 1.b), where σ_{eq} is the equilibrated stress—i.e. $\sigma_{eq} = \sigma(t \to \infty)$. We can obtain a piecewise spline-based analytical function $\sigma_{neq}(t)$ from the experimental measurement pairs $\{\hat{t}, \hat{\sigma}_{neq}\}$. From the instantaneous and quasistatic response curves (see Figure 1.a) we can also obtain within the spline context $\sigma_{neq}(E_e)$ and then $E_e(\sigma_{neq})$. As a result we can eliminate the stress variable σ_{neq} through $E_e(\sigma_{neq}(t)) = E_e(t)$. Once we have the function $E_e(t)$ in spline form, it is immediate to obtain $\dot{E}_e(t)$. Finally, from Eq. (29)

$$
\eta^d(\|\mathbf{E}_e(t)\|) = -\frac{\sigma_{neq}(t)}{3\dot{E}_e(t)} \quad (31)
$$

where the spline-based function $\eta^d(\|\mathbf{E}_e\|)$ is built with the pairs $\{\sqrt{3}E_e/2, -\sigma_{neq}/(3\dot{E}_e)\}$, where $E_e(t)$, $\sigma_{neq}(t)$ and $\dot{E}_e(t)$ are known for each experimental time measurement t. If we want to know the relaxation time function $\tau(\|\mathbf{E}_e\|)$ that governs the relaxation of stresses, see Eq. (30), then

$$
\tau(\|\mathbf{E}_e\|) = \frac{2\eta^d(\|\mathbf{E}_e\|)}{\omega_{neq}''(\mathbf{E}_e)} \quad (32)
$$

where $\omega_{neq}''(\mathbf{E}_e)$ is the second derivative of the Valanis-Landel term respect to the logarithmic strains $\mathbf{E}_e$. As aforementioned, the consideration of the dependence $\eta^d(\|\mathbf{E}_e\|)$ in the computational models of Refs. [20] and [21] would imply the modification of the computational algorithm (i.e. the consistent tangents) because $\mathbf{E}_e$ is continuously evolving.

A simplified approximation procedure used in the examples below, which requires neither the interpolation procedure nor the algorithm modification, but still captures to an excellent accuracy the stress-strain behavior and the strain-level dependency, may be obtained just assuming that $\eta^d(\|\mathbf{E}_e\|)$ depends only on the initial peek value $\mathbf{E}_e^0 = \mathbf{E}_e(t = 0^+)$ and then it preserves its value η_0^d for $t > 0^+$. In that case, from Eq. (31)

$$
3\eta_0^d = -\frac{\sigma_{neq}^0}{\dot{E}_e^0} = -\frac{\sigma_{neq}^0}{\dot{\sigma}_{neq}^0/Y_{neq}^0} = \frac{Y_{neq}^0 \sigma_{neq}^0}{\sigma_{neq}^0/\tau^0} = \tau^0 Y_{neq}^0 \quad (33)
$$

where

$$
Y_{neq}^0 = \frac{d\sigma_{neq}(E_e)}{dE_e}\bigg|_{E_e^0} \quad (34)
$$

and the relaxation time parameter τ^0 is obtained immediately as shown in Figure 1. In terms of the time parameter t^0 also shown in Figure 1

$$3\eta_0^d = \frac{t^0 Y_{neq}^0}{1 + \hat{\sigma}^0} \tag{35}$$

where $\hat{\sigma}^0 = \sigma_{eq}^0 / \sigma_{neq}^0$. For the initial state at $t = 0^+$, $E_e^0 \approx E^0$, so we can readily compute the test-specific values $\sigma_{eq}^0(E^0)$, $\sigma_{neq}^0(E^0)$ and $Y_{neq}^0(E^0)$. Measuring $t_0(E^0)$, Equation (35) gives the strain-level-dependent values of $\eta_0^d(E^0)$, which remain constant during the respective relaxation tests.

Finally, assume a material with proportional equilibrated and nonequilibrated strain energies, the case obtained in QLV and formulations based on the Simó framework. Then the stress ratio $\hat{\sigma}^0 = \sigma_{eq}^0 / \sigma_{neq}^0$ no longer depends on E^0 and takes the constant value $\hat{\sigma}^0 = Y_{eq}/Y_{neq}$, with Y_{eq} and Y_{neq} being the small strain Young moduli of the respective contributions to stress. If we additionally assume that η^d is constant, we arrive at

$$t^0 \propto \frac{1}{Y_{neq}^0} \propto \frac{1}{Y^0} \tag{36}$$

so the time parameter t^0 shown in Figure 1 would necessarily result inversely proportional to the initial uniaxial stiffness of the instantaneous response $Y^0 = d\sigma(E)/dE|_{E^0}$. This dependence is not observed, for instance, in the experiments performed in abdominal muscle simulated below.

4.2   Orthotropic case

Following analogous steps for uniaxial relaxation tests in preferred material axes of an orthotropic material, after some straightforward but lengthy algebra, we arrive at the following set of equations from which we can determine the three axial initial-strain-dependent viscosities η_{11}^d, η_{22}^d and η_{33}^d — cf. Eq. (97) in Ref. [21]

$$\begin{cases} 2\dfrac{Y_{11}^{neq}}{\eta_{11}^d} + \dfrac{H_{12}^{neq}}{\eta_{22}^d} + \dfrac{H_{13}^{neq}}{\eta_{33}^d} = \dfrac{9}{t_{11}^0 Y_{110}^{neq}/Y_{11}^{neq}} \left(1 + \dfrac{Y_{11}^{eq}}{Y_{11}^{neq}}\right) \\[2ex] \dfrac{H_{21}^{neq}}{\eta_{11}^d} + 2\dfrac{Y_{22}^{neq}}{\eta_{22}^d} + \dfrac{H_{23}^{neq}}{\eta_{33}^d} = \dfrac{9}{t_{22}^0 Y_{220}^{neq}/Y_{22}^{neq}} \left(1 + \dfrac{Y_{22}^{eq}}{Y_{22}^{neq}}\right) \\[2ex] \dfrac{H_{31}^{neq}}{\eta_{11}^d} + \dfrac{H_{32}^{neq}}{\eta_{22}^d} + 2\dfrac{Y_{33}^{neq}}{\eta_{33}^d} = \dfrac{9}{t_{33}^0 Y_{330}^{neq}/Y_{33}^{neq}} \left(1 + \dfrac{Y_{33}^{eq}}{Y_{33}^{neq}}\right) \end{cases} \tag{37}$$

where the small strain Young moduli Y_{ii}^{neq} and the coupling moduli H_{ij}^{neq} ($i \neq j$) are given as a function of $\mu_{ii}^{neq} = \frac{1}{2}\omega_{neq\,ii}''(\mathbf{0})$ and the Poisson ratios $\nu_{ij}^0 = -dE_j/dE_i|_0$, e.g.

$$\begin{cases} Y_{11}^{neq} := 2\mu_{11}^{neq} + \mu_{22}^{neq}\nu_{12}^0 + \mu_{33}^{neq}\nu_{13}^0 \\ H_{12}^{neq} := \mu_{11}^{neq} + 2\mu_{22}^{neq}\nu_{12}^0 - \mu_{33}^{neq}\nu_{13}^0 \\ H_{13}^{neq} := \mu_{11}^{neq} - \mu_{22}^{neq}\nu_{12}^0 + 2\mu_{33}^{neq}\nu_{13}^0 \end{cases} \tag{38}$$

These equations take a similar form to the ones obtained in Ref. [21] for strain-independent viscosities, but considering in the present case the modified values $t_{ii}^0 Y_{ii0}^{neq}/Y_{ii}^{neq}$,

$i = 1, 2, 3$, with Y_{ii0}^{neq} being the instantaneous (finite strain) moduli at $t = 0^+$.

5   Examples

Just as demonstrative examples of the application of the foregoing procedure in soft biological tissues, we reproduce in this section several relaxation responses of rabbit abdominal muscle that have been reported in Ref. [10].

5.1   Two single stress-relaxation curves in two perpendicular directions

We reproduce in this example the viscoelastic behavior of oblique muscles shown in Figure 6 of Ref. [10]. First, the instantaneous (i.e. equilibrated plus non-equilibrated) and relaxed (i.e. equilibrated) uniaxial responses in two perpendicular directions that are shown in Figure 6.a of Ref. [10] are exactly captured (i.e. to any desired precision) with our transversely isotropic hyperelastic model, as we show in Figure 2.a. The resulting axial terms of the computed instantaneous and equilibrated strain energy functions are shown in Figure 2.b.

On the other side, we can measure the time parameters $t_{11}^0 = t_T^0$ and $t_{33}^0 = t_L^0$ from Figure 6.b in Ref. [10], yielding approximately

$$t_{11}^0 = 65\,\mathrm{s} \ , \quad t_{33}^0 = 40\,\mathrm{s} \tag{39}$$

From Figure 6.b in Ref. [10] we can also measure the ratios between the instantaneous ($t = 0^+$ s) and relaxed ($t = 1500$ s) uniaxial stresses in both directions, from which by direct comparison with Figure 6.a in Ref. [10] (or with Figure 2), we obtain that the relaxation in direction 1 (transverse) corresponds to $\lambda_{11}^0 = 1.2$ and the relaxation in direction 3 (longitudinal) corresponds to $\lambda_{33}^0 = 1.3$. With λ_{11}^0 and λ_{33}^0 we can compute Y_{110}^{neq} and Y_{330}^{neq}. Once we have obtained the equilibrated and non-equilibrated strain energy functions, the time parameters t_{11}^0 and t_{33}^0 and the initial non-equilibrated stiffness values Y_{110}^{neq} and Y_{330}^{neq}, we can solve the system of equations of Eq. (37) particularized to the transversely isotropic case. We obtain the approximate solution

$$\eta_{11}^d = 1.495\,\mathrm{MPa\,s} \ , \quad \eta_{33}^d = 2.946\,\mathrm{MPa\,s} \tag{40}$$

which give the *preferred* relaxation times of our viscoelasticity model—cf. Ref. [21]

$$\tau_{11} = 399\,\mathrm{s} \ , \quad \tau_{33} = 301.6\,\mathrm{s} \tag{41}$$

We show in Figure 3.a the time-dependent responses that our model predicts for both uniaxial relaxation tests using the previously computed strain energies and relaxation times. We can observe the excellent agreement between the computed curves and the experimental ones using just one Maxwell element —compare with the predictions given by the model in Ref. [10], which we show in Figure 3.b for the reader convenience. Importantly, we remark that we have not used any optimization procedure in order to determine any component,
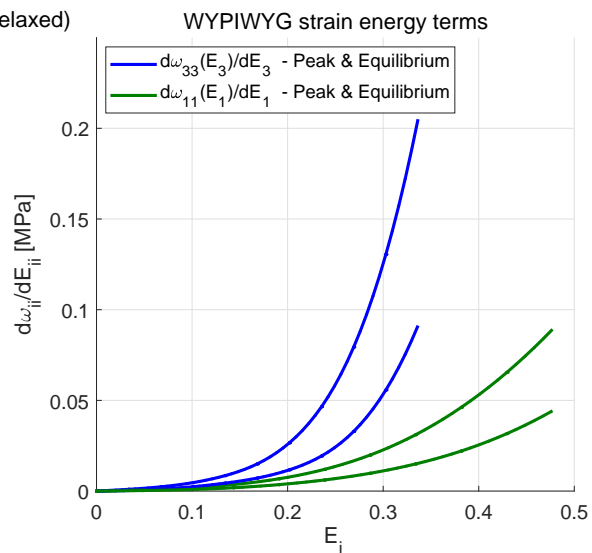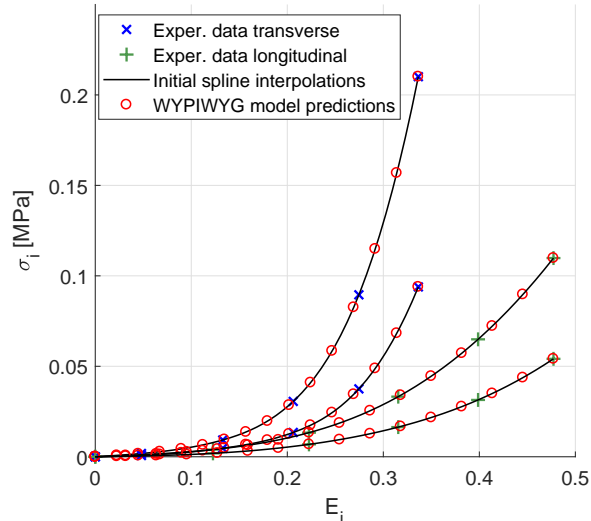
Fig. 2. Left (a): Predictions for the peak and relaxed behaviors in Fig6a of [10]. Right (b): WYPiWYG strain energy terms for the instantaneous (equilibrated + nonequilibrated) and equilibrated responses.
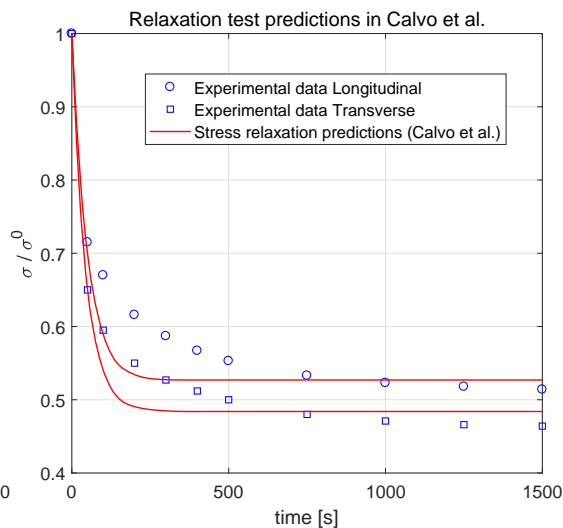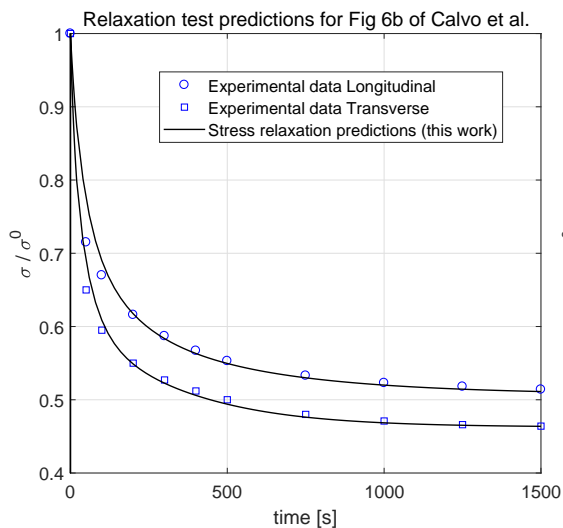

Fig. 3. Left (a): Stress relaxation predictions for the experimental data of Fig6b of [10] (longitudinal and transverse specimens). Right (b): Stress relaxation predictions using the model in [10] (redrawn from Fig6b of [10]).

whether elastic or viscous, of our non-linear viscoelasticity model. We have fully determined our model by direct resolution of the corresponding governing equations in each case yielding a unique solution for each model component; exactly as one would proceed in the infinitesimal case. In this case the viscosity parameters have no strain dependence according to experimental data in [10]. The reader can compare the shape of our predictions in Figure 3.a to those in Figure 3.b (redrawn from Figure 6 of Ref. [10]). The relevance of considering a non-equilibrium formulation, with fully non-linear evolution equations, instead a quasi-equilibrium formulation, with linear evolutions, is now apparent. The quasi-equilibrium viscoelasticity model is not capable of capturing the shape of the experimental curve of the relaxation test with one Maxwell element, whereas non-equilibrium viscoelasticity captures it naturally.

5.2 Several stress-relaxation curves in the same direction

We reproduce in this example the different stress-relaxation responses that rectus abdominis muscle experiences at different initial deformation levels, as shown in Figure 4 of Ref. [10]. In this case, only the responses in one material direction are known, so we use the isotropic model in the calculations.

We show in Figure 4.a the instantaneous (i.e. equilibrated plus non-equilibrated) and relaxed (i.e. equilibrated) uniaxial responses of the biological material under study. Since the curves in Figures 4.a and 4.b of Ref. [10] are inherently related, recall Figure 1, in this case we have extracted from Figure 4.a of Ref. [10] the instantaneous response and from Figure 4.b of Ref. [10] the relaxed-to-instantaneous stress ratios $\bar{\sigma}(E^0) = \sigma_{eq}^0/\sigma^0$ associated to each deformation level. For subsequent use, the relaxed-to-instantaneous stress
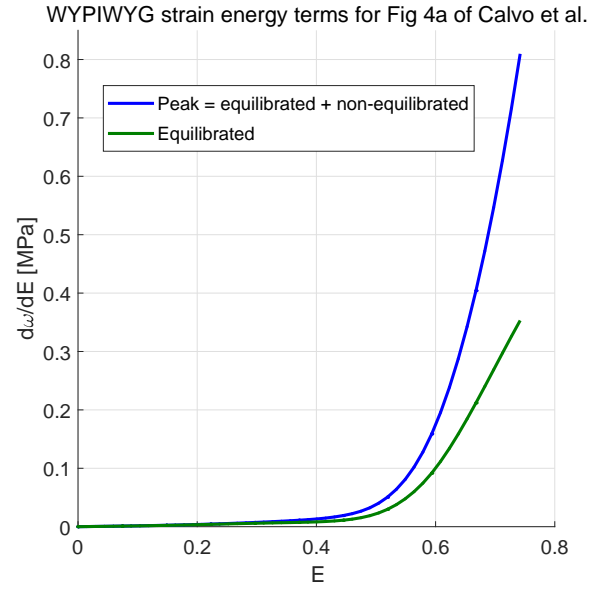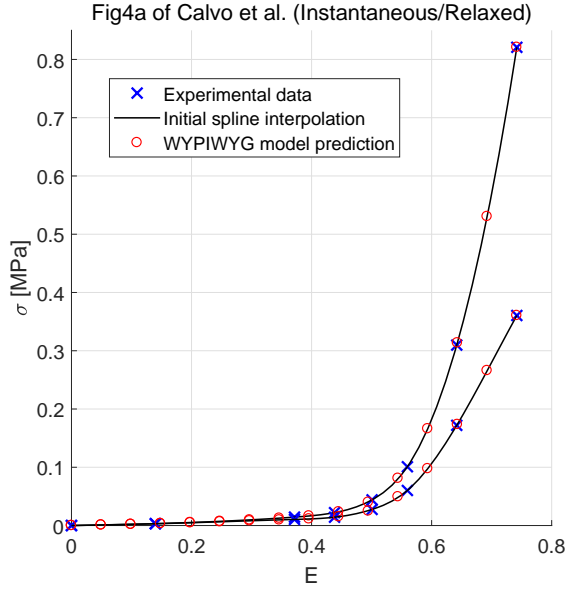
Fig. 4. Left (a): WYPiWYG hyperelastic predictions for the instantaneous (equilibrated + nonequilibrated) and relaxed (equilibrated) responses of the experiments in Figure 4a of [10]. Right (b): WYPiWYG stored energy terms for the instantaneous (equilibrated + nonequilibrated) and relaxed (equilibrated) responses of the experiments in Figure 4a of [10].
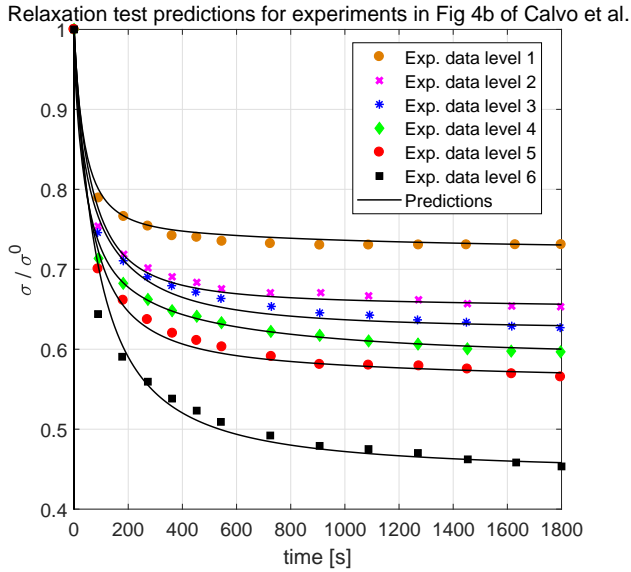

Fig. 5. Predictions for the relaxation tests performed at different stress levels. Experimental data redrawn from Figure 4b of [10].

ratios $\bar{\sigma}(E^0)$ relate to the initial-strain-dependent parameter $\hat{\sigma}(E^0)$ used in Eq. (35) through

$$\hat{\sigma}(E^0) = \frac{\sigma^0_{eq}}{\sigma^0_{neq}} = \frac{\sigma^0_{eq}}{\sigma^0 - \sigma^0_{eq}} = \frac{\sigma^0_{eq}/\sigma^0}{1 - \sigma^0_{eq}/\sigma^0} = \frac{\bar{\sigma}(E^0)}{1 - \bar{\sigma}(E^0)} \quad (42)$$

Again, we exactly capture both uniaxial responses using the isotropic spline-based hyperelastic formulation, as we show in Figure 4.a. The resulting first derivative functions of the instantaneous and relaxed Valanis–Landel terms are shown in Figure 4.b.

On the other hand, from Figure 4.*b* of Ref. [10] we can also measure the time parameters $t^0(E^0)$ associated to each initial deformation level E^0. We take them approximately as $t^0(E^0) = 100\,\text{s}$ for the six levels. Recall that by Eq. (35) this implies an initial-strain-dependent viscosity. Thereafter, we calculate the *initial-strain-dependent* deviatoric viscosity $\eta_0^d\left(E^0\right)$ following the procedure detailed above.

We show in Figure 5 the time-dependent responses that our modified model predicts for the different relaxation tests performed at different deformation levels using the calculated strain energies and the deformation-dependent deviatoric viscosity $\eta_0^d\left(E^0\right)$. Again, we can observe the excellent agreement between the computed curves and the experimental ones —cf. Figure 7 in Ref. [10] and note that we took the experimental data for our simulations from Figure 4 in Ref. [10]

6 Conclusions

Many soft biological tissues present a relevant strain-dependent viscous behavior which results in normalized relaxation curves which are different at different stress levels. The popular Quasilinear Viscoelasticity and the formulations based on the Simó framework result in a strain-independent behavior which is a consequence of the resulting direct relation between instantaneous and quasistatic behavior, as well as the direct relation between total stored energy and dissipation. The flow evolution equations are linear differential equations. The introduction of ad-hoc strain-dependent material parameters in Prony series, as for example in Ref. [10], allows for strain-dependent relaxation behavior. However, despite of employing optimization algorithms to perform a best-fit of material parameters to experimental data, relaxation curves are not satisfactorily captured.

In this work we present a procedure to naturally introduce strain-dependent viscous behavior through fully nonlinear evolution equations. Regarding the viscous behavior of

abdominal muscle, we show that excellent predictions are obtained at all strain levels, using both isotropic and anisotropic models. Instantaneous and quasistatic stored energies are exactly captured. The relaxation curves are also captured to a high accuracy using only the measured apparent relaxation time. The model is valid for arbitrarily large deviations from thermodynamic equilibrium and is amenable of efficient finite element implementation to predict the behavior under general deformations. The parameters, furthermore, are directly measured in experimental tests. As a main difference with other formulations, we obtain excellent predictions of the viscoelastic response of biological tissues using a single Maxwell element and anisotropic constitutive relations.

References

[1] Fung, Y.C., 2010. Biomechanics: Mechanical Properties of Living Tissues, 2nd. Ed. Springer, New York.

[2] Humphrey JD (2002) Cardiovascular Solid Mechanics: Cells, Tissues and Organs. Springer, New York.

[3] Duenwald SE, Vanderby R, Lakes RS (2009). Constitutive equations for ligament and other soft tissue: evaluation by experiment. Acta Mechanica 205:23-33.

[4] Van Loocke M, Lyons CG, Simms CK (2006) A validated model of passive muscle in compression. J Biomech 39: 2999-3009.

[5] Van Loocke M, Lyons CG, Simms CK (2008) Viscoelastic properties of passive skeletal muscle in compression: Stress-relaxation behaviour and constitutive modelling. J Biomech 41: 1555-1566.

[6] Van Loocke M, Simms CK, Lyons CG (2008) Viscoelastic properties of passive skeletal muscle in compression—Cyclic behaviour. J Biomech 42: 1038–1048.

[7] Simó JC (1987) On a fully three-dimensional finite-strain viscoelastic damage model: formulation and computational aspects. Comput Method Appl Mech 60(2):153–173.

[8] Simó JC, Hughes TJR (1998) Computational Inelasticity. Springer, Berlin.

[9] Peña E, Peña JA, Doblaré M (2008) On modelling nonlinear viscoelastic effects in ligaments. J Biomech 41: 2659–2666.

[10] Calvo B, Sierra M, Grasa J, Muñoz MJ, Peña E (2014) Determination of passive viscoelastic response of the abdominal muscle and related constitutive modeling: Stress-relaxation behavior. J Mech Behav Biomed Mater 36: 47–58.

[11] Holzapfel GA, Gasser TC (2001) A viscoelastic model for fiber-reinforced composites at finite strains: Continuum basis, computational aspects and applications. Comput Method Appl Mech Eng 190:4379–4403.

[12] Holzapfel GA (2000) Nonlinear Solid Mechanics: A continuum Approach for Engineering. Wiley.

[13] Kaliske M, Rothert H (1997) Formulation and implementation of three-dimensional viscoelasticity at small and finite strains. Comput Mech 19:228–239.

[14] Gültekin O, Sommer G, Holzapfel GA (2016). An orthotropic viscoelastic model for the passive myocardium: continuum basis and numerical treatment. Comp Meth Biomech Biomed Engrg, 19(15), 1647-1664.

[15] Reese S, Govindjee S (1998) A theory of finite viscoelasticity and numerical aspects. Int J Solid Struct 35(26):3455–3482.

[16] Haslach HW (2011) Maximum Dissipation Non-equilibrium Thermodynamics and its Geometric Structure. Springer, New York.

[17] Haupt P (1993) Thermodynamics of solids, in: W. Muschik (ed). Non-Equilibrium Thermodynamics with Applications to Solids, CISM Courses and Lectures (no. 336), Springer, Wien.

[18] Duenwald SE, Vanderby R, Lakes RS (2010). Stress relaxation and recovery in tendon and ligament: Experiment and modeling. Biorheology 47:1–14.

[19] Provenzano P, Lakes R, Keenan T, Vanderby R (2001). Nonlinear ligament viscoelasticity. Ann Biomed Engrg 29: 908-914.

[20] Latorre M, Montáns FJ (2015) Anisotropic finite strain viscoelasticity based on the Sidoroff multiplicative decomposition and logarithmic strains. Comput Mech 56: 503–531.

[21] Latorre M, Montáns FJ (2016) Fully anisotropic finite strain viscoelasticity based on a reverse multiplicative decomposition and logarithmic strains. Comput Struct 163: 56-70.

[22] Aranda-Iglesias D, Vadillo G, Rodríguez-Martínez JA, Volokh KY (2017) Modeling deformation and failure of elastomers at high strain rates. Mech Mater, 104, 85-92.

[23] Volokh KY (2016) Mechanics of Soft Materials. Springer, Singapore.

[24] Hoo Fatt MS, Ouyang X (2008) Three-dimensional constitutive equations for styrene butadiene rubber at high strain rates. Mech Mater, 40(1), 1-16.

[25] Sussman T, Bathe KJ (2009) A Model of Incompressible Isotropic Hyperelastic Material Behavior using Spline Interpolations of Tension-Compression Test Data. Commun Num Method 25:53–63.

[26] Latorre M, Montáns FJ (2014) What-You-Prescribe-Is-What-You-Get orthotropic hyperelasticity. Comput Mech 53(6):1279–1298.

[27] Crespo J, Latorre M, Montáns FJ (2017). WYPIWYG hyperelasticity for isotropic, compressible materials. Comput Mech 59(1): 73-92.

[28] Latorre M, Montáns FJ (2013) Extension of the Sussman–Bathe spline-based hyperelastic model to incompressible transversely isotropic materials. Comput Struct 122:13–26.

[29] Latorre M, Peña E, Montáns, FJ (2016) Determination and Finite Element Validation of the WYPIWYG Strain Energy of Superficial Fascia from Experimental Data. Ann Biomed Engrg, 1-12.

[30] Romero X, Latorre M, Montáns FJ (2017) Determination of the WYPiWYG strain energy density of skin through finite element analysis of the experiments on

circular specimens. Fin Elem Anal Des, 134, 1-15.

[31] Latorre M, Romero X, Montáns FJ (2016). The relevance of transverse deformation effects in modeling soft biological tissues. Int J Solid Struct, 99: 57-70.

[32] Latorre M, Montáns FJ (2017) WYPiWYG hyperelasticity without inversion formula: Application to passive ventricular myocardium. Comp Struct 185: 47-48.

[33] Murphy JG (2014). Evolution of anisotropy in soft tissue. Proc Royal Soc A, 470(2161): 20130548.

[34] Latorre M, Montáns FJ (2015) Material-symmetries congruency in transversely isotropic and orthotropic hyperelastic materials. Eur J Mech A-Solid 53:99–106.

[35] Dokos S, Smaill BH, Young AA, LeGrice IJ (2002). Shear properties of passive ventricular myocardium. Am J Physiol-Heart Circ Physiol, 283(6), H2650-H2659.

[36] Latorre M, Montáns FJ (2016) Stress and strain mapping tensors and general work-conjugacy in large strain continuum mechanics. Appl Math Model 40(5-6):3938–3950.

[37] Lubliner J (1985). A model of rubber viscoelasticity. Mech Res Commun, 12(2): 93-99.

[38] Purslow PP, Wess TJ, Hukins DWL (1998) Collagen orientation and molecular spacing during creep and stress-relaxation in soft connective tissues. J Exp Biol 201:135–142.